A New Approach to Partial Discharge Detection Under DC Voltage: Application to Different Materials

Pietro Romano, Antonino Imburgia, Giuseppe Rizzo, Guido Ala
L.E.PR.E. HV Laboratory, Department of Engineering,
Palermo University,
Palermo, Italy

Abstract

Understanding the propagation behavior of partial discharge signals across the branched cable joints helps significantly to improve the performance of condition monitoring and diagnostic solutions for medium voltage cable networks.

Index Terms — **HVDC, partial discharge, DC measurements, testing method**, **pattern recognition, discharge phenomena**

1 INTRODUCTION

In the last years the development of High Voltage Direct Current (HVDC) power transmission systems has pointed out some issues related to the assessment of their reliability [1-3]. In particular, due to the characteristics of the phenomenon, there is no consolidated method for measuring Partial Discharges (PDs) to identify insulation defects under DC stresses[4]. Despite the same phenomenon under AC stress, where the standard IEC 60270 is used [5], no technical standards have been developed for DC. In addition, with the same applied voltage magnitude, under constant voltage supply, the PD repetition rate is lower than under alternating voltage [6-7]. In other words, in order to identify a defect within the insulation, the DC voltage stress must be applied for a longer time than that under AC. Moreover, in order to identify the defect type, the phase-resolved-partial-discharge (PRPD) pattern which is helpful to identify the defect type, cannot be created under DC stress [8-11]. This is due to the constant shape of the DC stress, which not allows to assign a phase value to the discharge event but only the arrival time from t=0. In order to overcome these main problems related to the PD measurements under DC stress, some authors proposed new techniques mainly based on a DC voltage with superimposed periodic waveforms or ripples [12, 13]. Furthermore, some IEC Standards and Recommendations of IEEE and CIGRÈ have proposed test methods for HVDC extruded cables and accessories adopting PD measurement techniques suitable for AC [14-17]. This solution could give good results in terms of research of defects generated during fabrication process. On the contrary, under DC stress, the presence of space charge phenomena strongly influences the electric field distribution inside the dielectric and the discharge conditions dramatically change than that under AC [8]. For this reasons, the application of an AC wave shape could lead to approximate or incorrect results. With the aim to investigate the differences in PD measurements under AC and DC, a new waveform has been proposed by the authors in a previous work [18]. The new waveform is named Direct Current Periodic (DCP) and it is composed by both sinusoidal and constant part for a period. With the use of the DCP, it is possible to stress the specimen with the same effect as a pure DC voltage and detect PDs as with an AC waveform. Moreover, thanks to the sinusoidal part of the DCP waveform, it is possible to obtain the PD probe synchronization and therefore the generation of the PRDP pattern [18].

In the previous article, after describing the DCP waveform and the measurement setup, PD tests were performed on a Kapton specimen. The findings of that research show some interesting results in term of partial discharge inception voltage (PDIV) and repetition rate (PDRR). In particular, the PDIV results follow a second order polynomial law, depending on the parameter δ, going from 2.0 kV in AC to 14 kV in DC. At the same time, with the same variation's law, the PDRR decrease from 66 *PD/s* in AC to 0.084 *PD/s* in DC. Another finding, under the proposed DCP waveform, is the possibility to identify discharges in defects and discriminate simultaneous multiple phenomena as in AC.

In this paper, the above mentioned method has been extended to other polymeric materials, namely Cross-linked polyethylene (XLPE), Polyethylene terephthalate (PET) and to mineral oil Mass Impregnated (M.I.) paper. Measurements are also repeated again on Kapton specimens. Results confirm that polymeric materials have the same behavior, while M.I. paper differ slightly in terms of PDIV.

2 THE DC PERIODIC STRESS

The DCP waveform is developed and reported in detail in [18]. Here, a brief description is given. The DCP waveform is mathematically described in equation (1) and its shape, with positive and negative polarity, is shown in figures 1 and 2, respectively. The introduction, of the negative polarity in this work is due to the interest in reversal polarity phenomena in HVDC systems [19]. The DCP waveform follows a sinusoidal law from α to $\pi - \alpha$ and it is constant over the remainder of the period. Considering that δ can assumes values from -1 to +1, the parameter δV_x takes

values in the range $\pm V_x$. When $\delta = 0$, also $\alpha = 0$ and the waveform is sinusoidal for half period and zero for the rest. When $\delta = \pm 1$ the waveform coincide with pure DC with $\pm V_x$ amplitude. Therefore, by varying δ, the applied waveform assumes transient values from half AC wave to DC. Furthermore, for $\delta = \pm 0.625$ the RMS value of DCP coincides with the RMS value of an AC sinusoidal voltage with $\pm V_x$ amplitude.

$$v(t) = \begin{cases} V_x \sin(\omega t) & for\ \alpha \le \omega t \le \pi - \alpha \\ \delta V_x & for\ 0 \le \omega t < \alpha,\ \ \pi - \alpha < \omega t \le 2\pi \end{cases} \quad (1)$$

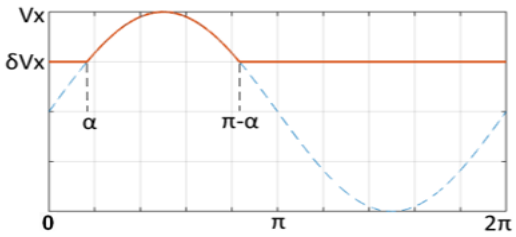

Figure 1: DCP waveform in positive polarity.

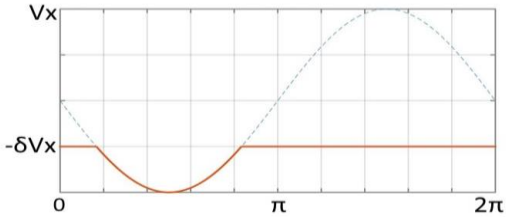

Figure 2: DCP Waveform in negative polarity.

Another fundamental aspect to describe is the comparison between DCP and DC in terms of space charge accumulation and its influence on the occurrence of PDs.

The evaluation of the charge accumulated at the interface between air and dielectric plays an important role in the establishment of conditions enhancing PDs. For this reason, the charge accumulated near the interface in case of periodic DC source has been compared to that occurring in case of pure DC source. By combining the current continuity equation, the Ohm's law for current density and the Gauss law for volumetric charge density, the space charge density can be calculated through the following equation:

$$\nabla \cdot (\varepsilon_0 \varepsilon_r E) = \rho \quad (2)$$

where E is the electric field, ε_0 is the vacuum permittivity, ε_r is the relative permittivity and ρ is the free volumetric charge density. The equation (2) has been numerically solved by applying the finite difference method. The interface thickness has been set equal to zero, therefore, the output value of ρ is dependent by the chosen spatial interval. However, the product between the spatial interval in the direction of the electric field and ρ returns the superficial density of charge. A simulation has been carried out for an air-XLPE sample with a peak voltage of the AC source equal to 5 kV and δ equal to 0.6. Then. the resulting superficial charge density has been compared with the calculated one by considering a pure DC source equal to 3 kV. In figure 3, the comparison between the resulting superficial charge densities *vs* time is shown. The accumulation of charge at the interface depends on the RMS value of the applied voltage. With reference to the above mentioned periodic DC voltage, the asymptotic value of superficial charge density is equal to that occurring if a 3,39 kV DC voltage is applied to the sample.

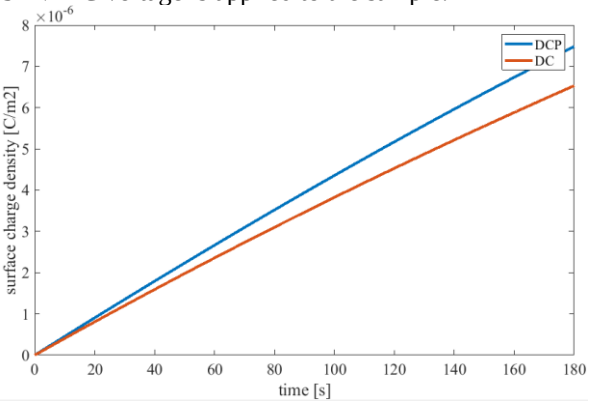

Figure 3: Accumulated surface charge density for 5 kV DCP with δ = 0.6 (blue line) and 3 kV DC (red line).

3 EXPERIMENTAL SETUP AND SPECIMENS UNDER TEST

The arranged measurement setup is reported in figure 4. The DCP waveform is generated by a code implemented in Matlab with positive or negative polarity and different δ values,. After its generation, the DCP waveform is sent to a signal generator whose maximum output voltage magnitude is equal to ±10 V. To increase the DCP voltage magnitude up to 1000 times, a Trek power amplifier is used. Finally, the amplifier output signal is applied to the specimen under test. In order to detect the PD phenomena, the Pry-Cam portable antenna sensor is adopted [20]. A synchronizer apparatus is connected to the TTL port of the function generator in order to read the generated DCP waveform frequency and synchronize the PD probe to create the PRPD pattern. The antenna sensor is also directly capable of synchronizing with the DCP waveform. The digital system is connected via Wi-Fi to a tablet for remote control and display of the acquired signals. The PRPD pattern, the time domain trend and the Fast Fourier Transform (FFT) of all acquired PD signals can be displayed and stored [20].

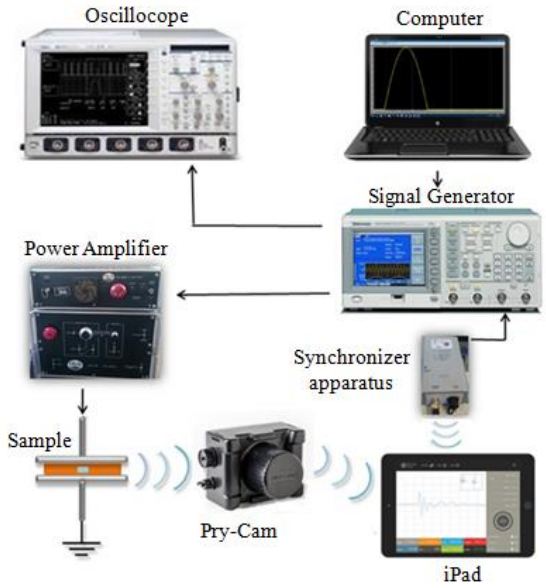

Figure 4: Experimental setup.

Test samples of different materials, are made of two layers of the same dielectric material. In the upper layer (the one in contact with the High Voltage electrode) a hole with 300 μm of diameter is made in order to create an air void defect and enhance internal discharges, as shown in figure 5. The two-layer asymmetrical configuration has been chosen instead of the more classic three-layer in order to reduce the partial discharge inception voltage (PDIV) and partially exceed limit of 10 kV of the power amplifier.

With the aim of investigating the behavior of materials subjected to DCP stress, and assess any differences with respect to Kapton's behavior, other two polymeric materials and one Mass Impregnated paper have been selected.

The cross linked polyetilene, XLPE, and the Mass Impregnated paper are mainly adopted in the cable industry. In addition, the polyetilene tetraflate, PET, is adopted in various electrical applications.

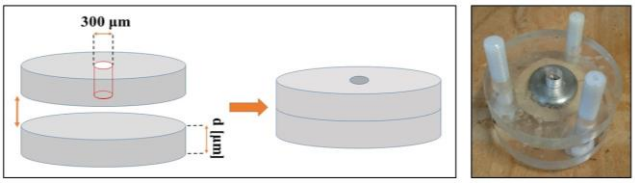

Figure 5: Specimen under test composed of two dielectric layers with thickness *d*. A hole is made in one foil in order to obtain internal PD.

For each material, the layer thickness d, the dielectric relative permittivity ε_r and the resistivity ρ, are reported in the Table I. Only for M.I. paper a third solid layer has been added to avoid breakdowns occurring with only two layers specimen.

Table I. Dielectric materials properties

Material	d $[\mu m]$	ε_r	ρ $[\Omega m]$
Kapton	127	2.24	$1 \cdot 10^{15}$
XLPE	90	2.23	$1 \cdot 10^{11}$
PET	110	3	$1 \cdot 10^{11}$
M.I. Paper	150	4.5	$4{,}7 \cdot 10^{11}$

4 TEST PROCEDURE AND EXPERIMENTAL RESULTS

The specimens listed in Table I have been subjected to both 50 Hz AC and DCP waveforms. First, as a reference measurement, the AC stress has been applied and the PDIV value as well as the PRPD patterns have been recorded. Then, the same procedure has been carried out by applying the DCP stress. In this case, the PD acquisitions have been made for different δ values (from 0 to 1 by step of 0.2) and for both voltage polarities. For each PD test, after detecting the PD inception voltage, the acquisition has been stopped at stabilized PDRR values. After each PD measurement, the specimens have been short circuited in order to remove the accumulated charges, which otherwise would have compromised the subsequent measures.

In the next paragraphs, the experimental results for Kapton, XLPE and PET specimens are reported in detail, whilst the findings for M.I. paper specimens have been described more synthetically in the Discussion. This is because, apart from PDIV, the other results are substantially similar to those of the other materials...

4.1 Kapton

Measurements of PDs occurring in Kapton specimens have been repeated in order to confirm the results obtained in the previous paper [18]. As specified in the introduction part of the paragraph, first, the AC measurements have been done as starting reference parameters. Then, the DCP tests with increasing values of δ for both polarities have been performed.

- *AC test.* PD Measurement under AC voltage shows a standard internal behaviour with high PD amplitude variability and left inception phase angle shift with voltage increase. The PDIV has been detected at 1.4 kV and the correspondent PRPD pattern is shown in figure 6. The brackets $\Delta\Phi_+$ and $\Delta\Phi_-$ represent the widths of the spectrum for positive and negative PDs, respectively.

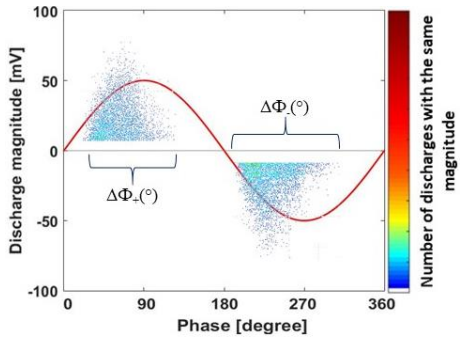

Figure 6: PRPD Pattern under 1.4 kV 50 Hz AC stress. $\Delta\Phi_+$ and $\Delta\Phi_-$ are the width of the spectrum for positive and negative PDs, respectively.

In order to verify that the AC waveform provides the same PD signal as that due to a DCP stress, in term of pulse time and frequency domain trend, an acquired PD pulse and its frequency spectrum have been reported in figures 7 and

8, respectively. The pulse shape of figure 7 have a typical second order response and the first two oscillations last about 130 nanoseconds. In the frequency spectrum of figure 8 the highest frequency is about 5 MHz.

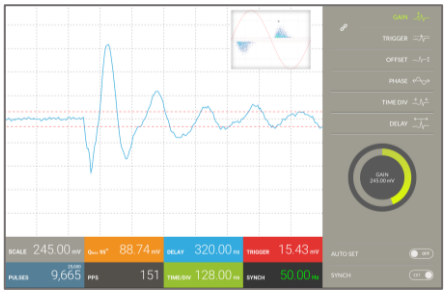

Figure 7: Time domain PD pulse detected under AC stress.

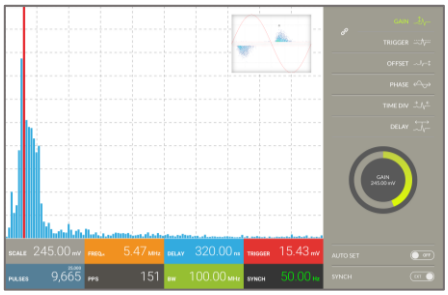

Figure 8: Frequency spectrum of the PD pulse under AC stress.

- *DCP tests*. By applying the DCP waveform with positive polarity and δ=0, the detected PDIV results 2.2 kV and the obtained PRPD pattern is shown in figure 9.

By making a comparison between the PRPD pattern of the sinusoidal stress of figure 6 and the PRPD pattern of the DCP some considerations can be made. Some of these have been already discussed in the previous paper as the presence of both negative and positive discharges. In particular, the pattern of figure 9 shows a reduction in the width of discharge pulse phase, thus the values of $\Delta\Phi_+$ and $\Delta\Phi_-$ are lower. Furthermore, positive discharges stop before the *dv/dt* equal to zero and negative discharges start and stop before the zero crossing.

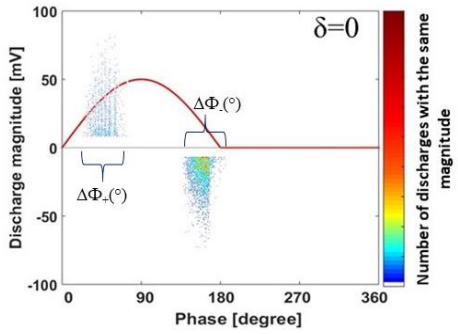

Figure 9. PRPD Pattern under 2.2 kV 50 Hz DCP positive polarity with δ=0. $\Delta\Phi_+$ and $\Delta\Phi_-$ are the width of the spectrum for positive and negative PDs, respectively.

By making a comparison between the PRPD pattern of the sinusoidal stress of figure 6 and the PRPD pattern of the DCP some considerations can be made. Some of these have been already discussed in the previous paper as the presence of both negative and positive discharges. In particular, the pattern of figure 9 shows a reduction in the width of discharge pulse phase, thus the values of $\Delta\Phi_+$ and $\Delta\Phi_-$ are lower. Furthermore, positive discharges stop before the *dv/dt* equal to zero and negative discharges start and stop before the zero crossing.

Despite some differences are evident in the PRPD patterns of the AC and DCP cases strictly related to the different waveforms, some similarities are noteworthy. In particular, the detected PD pulse characteristics under AC stress, previously reported in figures 7 and 8, are almost the same as those found with the DCP stress. In figure 10, an acquired PD pulse under DCP stress is shown. The time domain response is perfectly identical than that under AC stress as well as the frequency spectrum. This confirms that the PD pulse characteristics are more related to the geometry of the defect than to the applied stress [20, 21].

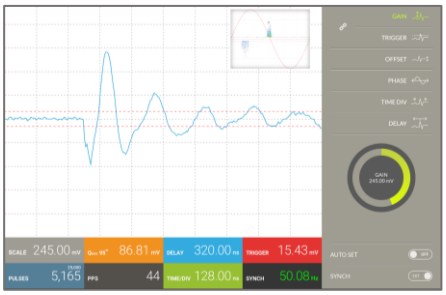

Figure 10: Negative PD pulse detected under DCP stress with δ=0.

Subsequently, by varying the parameter δ of the DCP waveform, the PRPD patterns have been obtained. Considering their similarity with those of the previous work, here only the PD features, summarized in Tables II and III, have been reported. As can be seen in [18], the more δ increases, the more the width of the spectrum $\Delta\Phi$ decreases, as well as the number of discharge pulses. Then, the DCP waveform with negative polarity has been applied as voltage stress and the PRDP patterns for δ equal to 0 and 0.6 are shown in figure 11. For δ = 0.8 a very low number of PDs have been detected, while for δ = 1, no PD events have been measured.

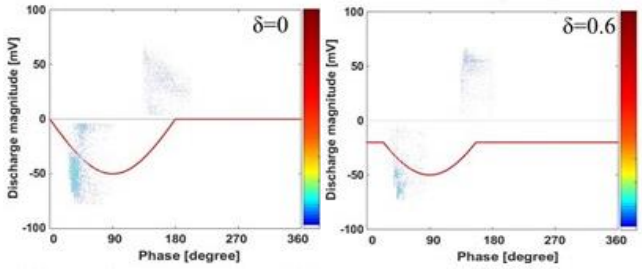

Figure 11: PRPD pattern acquired under the negative DCP waveform, for δ values 0 and 0.6, in the Kapton specimen.

The differences in the pattern shape, between the tests with positive and negative polarity are mainly due to the different dielectric properties of the radiating surface. In fact, under positive polarity, the electrons are provided by the electrode-air interface whilst, under negative polarity, the electrons are provided by the air-Kapton interface. Under negative polarity it is also possible to notice that a certain amount of discharges is present in the constant part of the applied waveform. This

phenomenon could be interpreted as analogous to what is called "echo PD", which is explained in detail in [22].

Regardless of the voltage polarity, it can be observed that when δ increases, the sinusoidal part of the DCP waveform decreases as well as the *dv/dt*. This mainly causes a decrease of the PDRR and a reduction of the width of the spectrum $\Delta\Phi$ for both polarities discharges. In addition, when δ increases, the DCP looks more and more like the DC shape, therefore the PDIV increases. Under AC and DCP wavefoms, the detected PDIV and PDRR, also called with the acronym PPS (pulse per second), are summarized in Table II with diefferent δ values for positive and negative polarity.

Table II: Kapton specimen. PD features detected under AC and DCP test for positive and negative polarity for different values of δ.

δ	PDIV-DCP [kV]		PPS-DCP [PD/s]		PDIV-AC [kV]	PPS-AC [PD/s]
	+	-	+	-		
0.0	2.8	2.4	38	55	1.4	140
0.2	3.4	3.0	22	32		
0.4	4.2	3.9	16	23		
0.6	6.1	6.0	10	12		
0.8	10	8.3	2	3		
1.0*	14.28	11.46	0.4	0.8		

* *Solutions of polynomial equations for $\delta = 1$.*

It can be noted that the PDIV almost doubles from AC to DCP with δ = 0 and, at the same time, the PPS decreases by about one third. The complete correlation between the PDIV and the parameter δ of the DCP waveform is shown in figure 12, which illustrates the second order polynomials that adapt the experimental results of PDIV *vs* δ under positive and negative DCP stress.

The following polynomial formulas are the simplest mathematical expressions that fit to experimental data:

$$PDIV = 13.75\delta^2 - 2.45\delta + 2.98 \quad (3)$$

$$PDIV\_ = 8{,}21\delta^2 + 0{,}83\delta + 2{,}42 \quad (4)$$

Where the correlation coefficients R^2 are equal to 0.99.

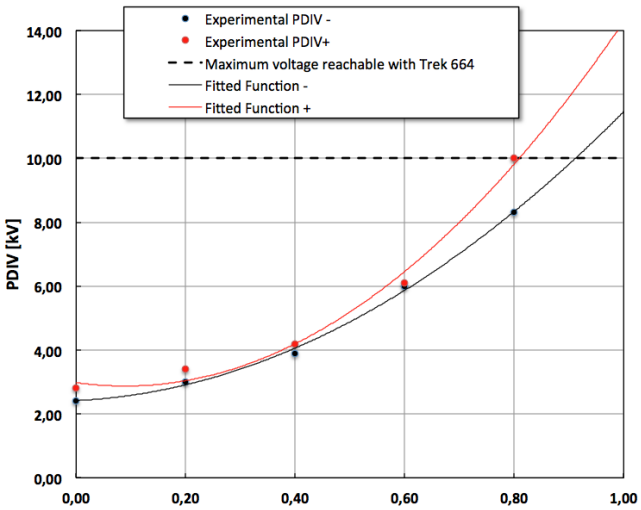

Figure 12: Experimental PDIV *vs* δ for Kapton specimen for positive polarity (red circles) and negative polarity (black circles) and the second order polynomials in δ fitted to the experimental data (solid red and black lines).

The parabolic trend of the curve is useful for determining the tendency in the value of PDIV in DC. This is because for δ greater than 0.8 the PDIV is greater than 10 kV, which is the maximum voltage level provided by the amplifier used in our measurement setup. This result is in line with what was previously achieved in [18]. As it can be observed, in both cases, the PDIV at constant DC voltage (DCP with δ = 1) is approximately 14 kV. For the other values of δ, the offset between the two curves is very small. It is likely that this difference is due to the different acquisition systems used in the two works, namely Pry-Cam prototype previously and portable Pry-Cam in the present paper.

The experimental results under DCP negative polarity show substantially the same trend as that under positive polarity, although the PDIV in the former case tends to be 2.8 kV lower than in the latter.

For Kapton, the PPS values also follow a second order polynomial trend. The findings of this case are reported in Table II.

4.2 XLPE

The second material to be tested is cross-linked polyethylene, called XLPE for cable applications. Its structure provides pronounced resistance to abrasion, stress, chemicals and temperature. In addition, since XLPE does not contain chloride, like PVC, it is more environmentally friendly. The same study and experimental tests, made for the Kapton specimen, have been performed for the XLPE sample. The acquired AC and DCP PRPD patterns for positive polarity, and DCP PRPD patterns for negative polarity, are reported in figures 13 and 14, respectively. Contrary to what has been observed for the Kapton specimen, in this case, for AC voltages and for low values of δ, the traditional "rabbit ear" of internal PDs is visible. This phenomenon is evident above all for the positive discharges where the discharges are extinguished naturally as the *dv/dt* decreases both in AC and in DCP. A different behavior can be observed with negative discharges. In AC case, negative discharges occur near the zero crossing of the voltage and show the same "rabbit ear" behavior than that in the positive one. In DCP case, negative discharges stop at $\pi-\alpha$ phase angle when the waveform transits from sinusoidal to constant shape. The differences in the pattern shape of the two specimens, Kapton and XLPE, are mainly due to the different dielectric material properties.

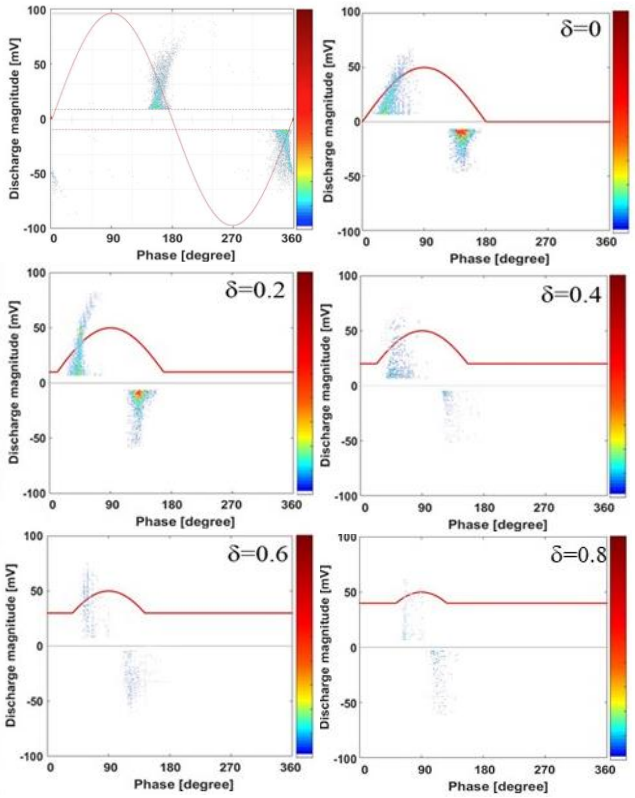

Figure 13: PRPD patterns acquired under AC and positive DCP waveforms, for different values of δ, in the XLPE specimen.

The negative DCP patterns show a behavior similar to that of positive ones. The most significant acquired patterns are reported in figure 14.

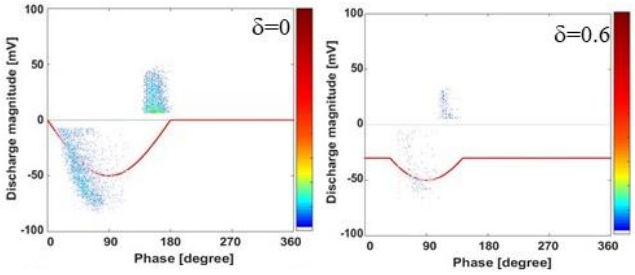

Figure 14: PRPD patterns acquired under negative DCP waveform, for different values of δ, in the XLPE specimen.

The features of the acquired PDs, under positive and negative polarity of the DCP waveform, are summarized in Table III.

By comparing with the results found for the Kapton specimen, it can be noted that in AC, whilst the PDIV are almost the same, the PPS for the XLPE are less than 50% compared to Kapton. This highlights the XLPE's good resilience to partial discharges. Instead, δ-rated PDIV are on average lower than those of Kapton. Furthermore, unlike Kapton, no significant changes between the parameters detected for positive and negative polarity have occurred.

Table III: XLPE specimen. PD features detected under AC and DCP test for positive and negative polarity for different values of δ.

δ	PDIV-DCP [kV]		PPS-DCP [PD/s]		PDIV-AC [kV]	PPS-AC [PD/s]
	+	-	+	-		
0.0	2.2	1.9	15	20	1.6	60
0.2	2.9	3.0	5	15		
0.4	3.1	3.5	5	5		
0.6	4.7	5.1	5	2		
0.8	8.5	8.5	2	2		
1.0*	12.40	11.84				

* *Solutions of polynomial equations for $\delta = 1$.*

For XLPE material, the second order polynomial curves fitting PDIV results, plotted in figure 15, are given by:

$$PDIV_{+}=13{,}57\delta^2 - 3{,}66\delta+2{,}49 \quad (5)$$

$$PDIV_{-}=10{,}18\delta^2 - 0{,}49\delta+2{,}15 \quad (6)$$

Where the correlation coefficients R^2 are equal to 0.97.

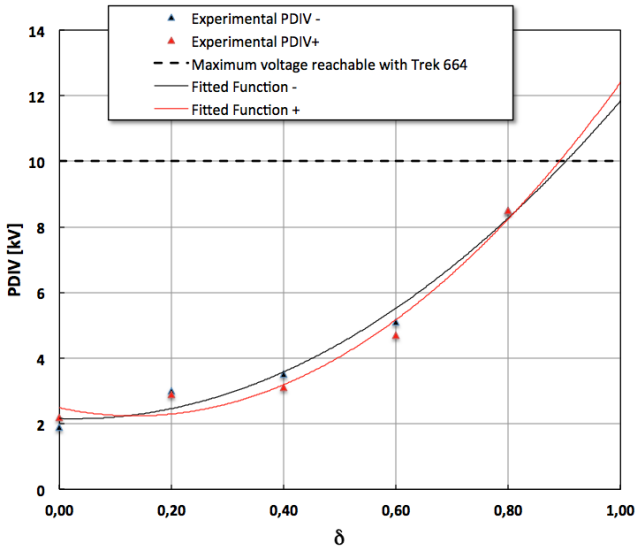

Figure 15: Experimental PDIV *vs* δ for XLPE specimen for positive polarity (red triangles) and negative polarity (black triangles) and the second order polynomials in δ fitted to the experimental data (solid red and black lines).

As it can be seen, for δ = 1, the PDIV was not detected experimentally because it exceeds 10 kV. In this case, the solution of the polynomial equation in δ gives a PDIV of approximately 12 kV, for both polarities. Unlike Kapton, however, in XLPE, the trend of the PPS does not follow a second order polynomial in δ. For this reason, table III does not show DC trend values.

4.3 PET

The PET films, due to their excellent characteristics as insulator, are usable in several electrical applications such as cable wrapping and motor insulation. The acquired AC and DCP PRPD patterns for positive and negative polarity, are reported in figure 16 and 17, respectively. Instead, in Table IV the main features of the detected PD are summarized.

As it can be seen in the obtained PRPD patterns, the "rabbit ear" shape is not visible, as for the Kapton sample. In addition, positive and negative parameters are very similar and often coincident.

The Polynomial second order fitting curves, plotted in figure 18, are given by:

$$PDIV+=13{,}57\delta^2 - 3{,}45\delta + 2{,}39 \quad (7)$$

$$PDIV\_=14{,}29\delta^2 - 3{,}83\delta + 2{,}40 \quad (8)$$

Where the correlation coefficients R^2 are equal to 0.98.

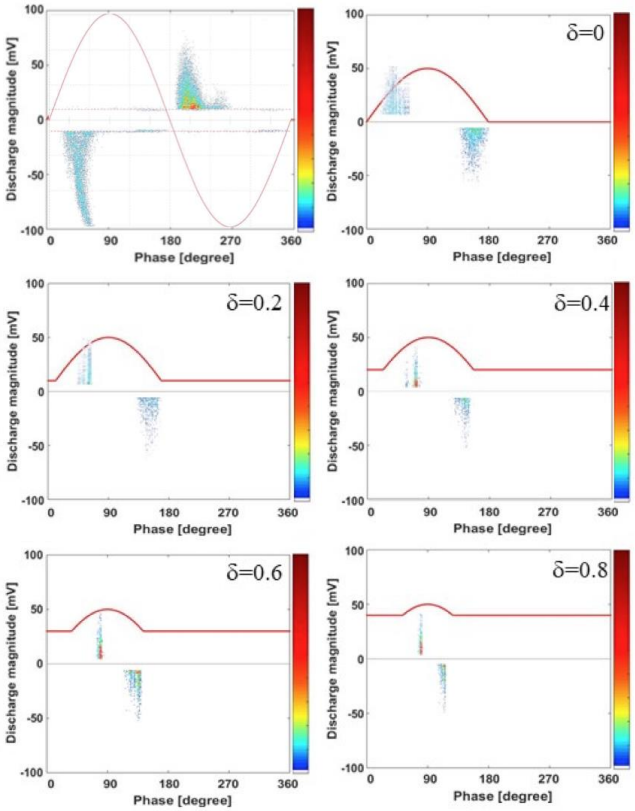

Figure 16: PRPD patterns acquired under AC and positive DCP waveforms, for different values of δ, in the PET specimen.

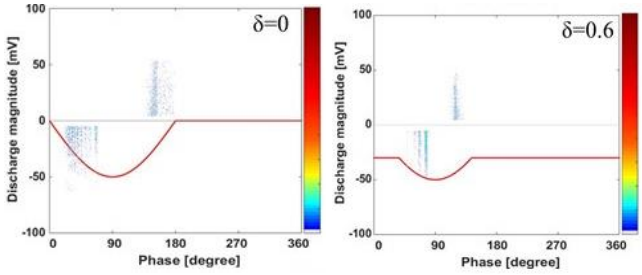

Figure 17: PRPD pattern acquired under the negative DCP waveform, for different values of δ, in the PET specimen.

Even for PET, for δ = 1, the PDIV has been not detected experimentally because it exceeds 10 kV. In this case, the solution of the polynomial equation in δ gives a PDIV of approximately 12.5 kV, for both polarities.

Table IV: PET PD features detected under AC and DCP test for positive and negative polarity for different values of δ.

δ	PDIV-DCP [kV]		PPS-DCP [PD/s]		PDIV-AC [kV]	PPS-AC [PD/s]
	+	-	+	-		
0.0	2.2	2.2	16	16	1.4	60
0.2	2.6	2.6	14	11		
0.4	3.2	3.2	14	10		
0.6	4.8	4.8	8	10		
0.8	8.5	8.7	6	7		
1.0*	12.51	12.86				

* *Solutions of polynomial equations for δ = 1.*

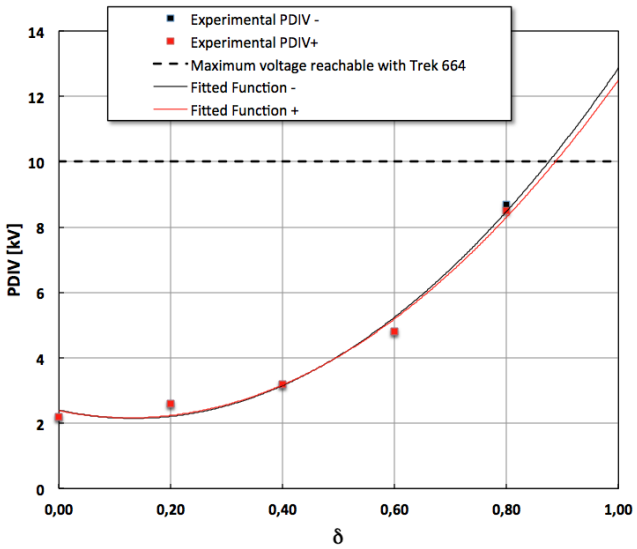

Figure 18: Experimental PDIV *vs* δ for PET specimen for positive polarity (red squares) and negative polarity (black squares) and the second order polynomials in δ fitted to the experimental data (solid red and black lines).

Unlike Kapton and as with XLPE, PPS values do not follow a second order polynomial in δ. For this reason, table IV does not show DC trend values.

5 DISCUSSIONS

As mentioned above, for the mass impregnated paper, the results are described in this paragraph. The M.I. paper shows a behavior similar to that of the other materials tested herewith some differences. The discharge phenomenon in AC has the typical behavior due to an internal void. The trend of PD pulses in time and frequency domain is almost superimposed on that of other materials. On the contrary, by applying DCP, no discharges with double polarity have been detected. This phenomenon has been confirmed under negative polarity where only negative discharges appear. This is probably due to the very low PPS rate. Raising up the voltage, this phenomenon disappears and discharges of both polarities appear again.

In order to compare the results for all materials, however, it is necessary to take into account some dimensional differences shown in Table I of 3rd paragraph. With differences in thickness of the layers and of the cavities, the results in terms of the PDIV trend are not directly comparable. Therefore, in order to compare the results, the value of the electric field applied inside the cavities has been determined. To do this, knowing the external PDIV, the voltage applied to the cavity boundaries has been calculated, through the simplified circuit models both in AC (capacitive model) and in DC (ohmic-capacitive model) for DCP [23, 24]. The obtained results are

shown in figures 19 and 20. As it can be noted in figure 19, for all the tested materials, the electric field depends on δ following a second order polynomial with a R^2 confidence of 0.97÷0.99.

Kapton and PET have very similar behavior while XLPE, after δ=0,4, differs from the other polymeric materials because the value of the electric field grows faster than the others. At the same time, the M.I. paper has a flatter pattern and with a lower slope than the other materials.

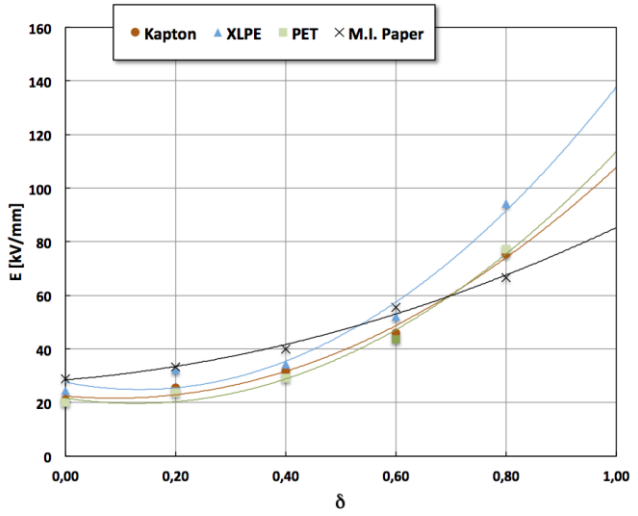

Figure 19: Comparison among the variation of electric field corresponding to the measured PDIV with δ and polynomial in δ fitted to the experimental data for positive polarity.

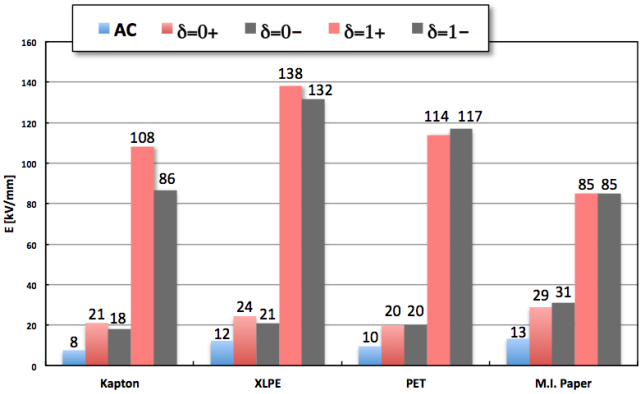

Figure 20: Comparison among the electric field corresponding to the measured PDIV in AC and with δ=0 and the tendency with δ=1 (DC) for positive and negative polarity.

In figure 20, a comparison among the different materials is shown in term of corresponding electric field at the Inception Voltages in AC and DCP with δ=0 for both polarities. In addition, δ=1 tendency values are also added in order to compare the experimental values obtained with the presumed DC values. First of all, the findings demonstrate a strong variation between Inception electric field values under AC and DC. Again from this figure, it is evident that all materials have a similar behavior in terms of electric field values varying from AC to DC. With AC, values vary from 8 kV/mm for the Kapton to 13 kV/mm for the M.I. paper with a 60% of variability. In DC, they pass from 85 kV/mm for the M.I. paper to 138 kV/mm for the XLPE, showing the same 60% of variability. However, in this case, the XLPE and the M.I. paper have the maximum and the minimum value, respectively. The M.I. paper has the slightest variation between maximum and minimum value whilst the Kapton has the maximum. In terms of resilience to partial discharges, XLPE shows the best results. With reference to the obtained experimental data reported in the previous paragraphs, it can be noticed that, for all specimens, the increasing of the parameter δ causes the increase of the PDIV, the reduction of the PPS and width of the spectrum, $\Delta\Phi_+$ and $\Delta\Phi_-$.

6 CONCLUSIONS

In order to overcome some issues related to the PD measurement under DC stress, a new type of waveform has been developed as described in a previous work. In that article, after introducing the DCP waveform, its performance has been verified in a Kapton sample and only in positive polarity. In this work, the DCP waveform in both polarities has been applied in other three dielectric samples, such as XLPE, PET and M.I. paper. Beyond this, the Kapton sample has been tested again in order to demonstrate the repeatability of the PD measure under DCP stress.

First of all, a numerical analysis demonstrates the similarity in terms of accumulated space charge at the interface between air and dielectric between DCP and DC. The similarities between all the tested specimen have been experimentally confirmed in terms of PRPD patterns and PD responses in time and frequency domain.

For all the specimens, the recorded PDIV and PPS have been reported, as well as the most relevant PRPD patterns acquired under the DCP waveform with different δ values. The obtained results show that the Kapton's behavior detected in the previous work is confirmed also for the other materials and the PDIV depends on δ parameter as a second order polynomial. In term of PPS, this trend is not confirmed in the same way. It is probably due to the reduced number of discharges detected at the inception voltages. Simultaneously, the width of the spectrum $\Delta\Phi_+$ and $\Delta\Phi_-$ and the phase distance between opposite polarity PD pulses are reduced. Similar results were obtained with negative polarity.

Due to the maximum voltage level of the measurement setup, the PDIV under the pure DC stress, has been not experimentally detected but analytically predicted. However, taking into account geometrical differences among specimens, corresponding electric field inside the cavities has been determined and a direct comparison has been performed. Results confirm a strong difference between experimental AC electric field, corresponding to internal PDIV, and that analytically predicted for a DC source. Moreover, XLPE shows the best results in term of resilience to the partial discharges.

In future works, these calculated PDIV values will be experimentally confirmed by adopting a suitable DC surce with higher voltage level. Fhurtermore, PD measurements will be performed by applyng DCP voltage supply for long time in order to evaluate the effect of space charge

accumulation at different time from the beginning of the tests.

REFERENCES

[1] G. Mazzanti; M. Marzinotto, "Improved Design of HVDC Extruded Cable Systems," in Extruded Cables for High-Voltage Direct-Current Transmission: Advances in Research and Development, 1, Wiley-IEEE Press, 2013.

[2] J. C. Fothergill, “The coming of Age of HVDC extruded power cables,” in 2014 IEEE Electrical Insulation Conference (EIC), 2014, pp. 124–137.

[3] P. Morshuis, A. Cavallini, D. Fabiani, G. C. Montanari, and C. Azcarraga, “Stress conditions in HVDC equipment and routes to in service failure,” IEEE Transactions on Dielectrics and Electrical Insulation, vol. 22, no. 1, pp. 81–91, 2015.

[4] P. Romano, R. Candela, A. Imburgia, G. Presti, E. R. Sanseverino and F. Viola, "A new technique for partial discharges measurement under DC periodic stress," 2017 IEEE Conference on Electrical Insulation and Dielectric Phenomenon (CEIDP), Fort Worth, TX, 2017, pp. 303-306.

[5] High-Voltage Test Techniques—Partial Discharge Measurements, IEC 60270:2000+AMD1:2015 CSV.

[6] P. Romano et al., "Partial Discharge Measurements under DC Voltages Containing Harmonics Produced by Power Electronic Devices," 2018 IEEE Conference on Electrical Insulation and Dielectric Phenomena (CEIDP), Cancun, 2018, pp. 558-561.

[7] A. Imburgia, P. Romano, F. Viola, N. Hozumi and S. Morita, "Partial discharges behavior under different rectified waveforms," 2017 International Symposium on Electrical Insulating Materials (ISEIM), Toyohashi, 2017, pp. 114-117.

[8] U. Fromm, “Interpretation of partial discharges at DC voltages,” IEEE Trans. Dielectr. Electr. Insul., vol. 2, no. 5, pp. 761–770, 1995.

[9] I. J. Seo, U. A. Khan, J. S. Hwang, J. G. Lee, and J. Y. Koo, “Identification of insulation defects based on chaotic analysis of partial discharge in HVDC superconducting cable,” IEEE Trans. Appl. Supercond., vol. 25, no.3, pp. 1–5, Jun. 2015.

[10] A. Pirker and U. Schichler, “Partial discharges at DC voltage—Measurement and pattern recognition,” in 2016 Int. Conf. Cond. Monit. Diagn. (CMD), 2016, pp. 287–290.

[11] H. Niu, A. Cavallini, G. Montanari, and Y. Zhang, “Noise rejection strategy and experimental research on partial discharge at DC voltage,” in 2009 IEEE 9th Int. Conf. Prop. Appl. Dielectr. Mater., 2009, pp. 489–492.

[12] M. A. Fard, A. J. Reid and D. M. Hepburn, "Analysis of HVDC superimposed harmonic voltage effects on partial discharge behavior in solid dielectric media," in IEEE Transactions on Dielectrics and Electrical Insulation, vol. 24, no. 1, pp. 7-16, Feb. 2017.

[13] M. A. Andrade et al., "Partial discharge behavior under single phase half and full-bridge rectifier," 2017 IEEE Conference on Electrical Insulation and Dielectric Phenomenon (CEIDP), Fort Worth, TX, 2017, pp. 393-396.

[14] G. Mazzanti et al., "The insulation of HVDC extruded cable system joints. Part 1: Review of materials, design and testing procedures," in IEEE Transactions on Dielectrics and Electrical Insulation, vol. 26, no. 3, pp. 964-972, June 2019.

[15] G. Mazzanti et al., "The insulation of HVDC extruded cable system joints. Part 2: Proposal of a new AC voltage PD measurement protocol for quality control during routine tests," in IEEE Transactions on Dielectrics and Electrical Insulation, vol. 26, no. 3, pp. 973-980, June 2019.

[16] CIGRE Working Group B1.32. Recommendations for Testing DC Extruded Cable Systems for Power Transmission at a Rated Voltage up to 500 kV. CIGRE Technical Brochure 496. Apr. 2012.

[17] [19] Power Cables with Extruded Insulation and Their Accessories for Rated Voltages Above 150 kV (Um 1/4 170 kV) up to 500 kV (Um 1/4 550 kV) Test Method and Requirements, 2nd ed., IEC 62067, Nov. 2011.

[18] P. Romano, G. Presti, A. Imburgia and R. Candela, "A new approach to partial discharge detection under DC voltage," in IEEE Electrical Insulation Magazine, vol. 34, no. 4, pp. 32-41, July-August 2018.

[19] M. A. Fard, M. E. Farrag, S. G. McMeekin and A. J. Reid, "Partial discharge behavior under operational and anomalous conditions in HVDC systems," in IEEE Transactions on Dielectrics and Electrical Insulation, vol. 24, no. 3, pp. 1494-1502, June 2017.

[20] P. Romano, A. Imburgia, G. Ala, “Partial discharge detection using a spherical electromagnetic sensor”, Sensors, vol. 19, no. 5, 2019.

[21] P. Romano et al., "Partial discharges at different voltage waveshapes: Comparison between two different acquisition systems," in IEEE Transactions on Dielectrics and Electrical Insulation, vol. 25, no. 2, pp. 584-593, April 2018.

[22] M. Florkowski, B. Florkowska, and P. Zydron, “Partial discharge echo obtained by chopped sequence,” IEEE Trans. Dielectr. Electr. Insul., vol. 23, no. 3, pp. 1294–1302, Jun. 2016.

[23] C. Pan, G. Chen, J. Tang and K. Wu, "Numerical modeling of partial discharges in a solid dielectric-bounded cavity: A review," in IEEE Transactions on Dielectrics and Electrical Insulation, vol. 26, no. 3, pp. 981-1000, June 2019.

[24] G. Ala, R. Candela, P. Romano and F. Viola, "Simplified hybrid PD model in voids," 8th IEEE Symposium on Diagnostics for Electrical Machines, Power Electronics & Drives, Bologna, 2011, pp. 451-455.

[25] M. Florkowski, B. Florkowska and R. Włodek, "Investigations on post partial discharge charge decay in void using chopped sequence," in IEEE Transactions on Dielectrics and Electrical Insulation, vol. 24, no. 6, pp. 3831-3838, Dec. 2017.